Cretaceous Research 38 (2012) 40–51

Contents lists available at SciVerse ScienceDirect

Cretaceous Research

journal homepage: www.elsevier.com/locate/CretRes

Stratigraphic transition and palaeoenvironmental changes from the Aptian oceanic anoxic event 1a (OAE1a) to the oceanic red bed 1 (ORB1) in the Yenicesihlar section, central Turkey

Xiumian Hu [a,*], Kuidong Zhao [a], Ismail Omer Yilmaz [b], Yongxiang Li [a]

[a] State Key Laboratory for Mineral Deposits Research, School of Earth Sciences and Engineering, Nanjing University, Hankou Road 22, Nanjing 210093, China
[b] Department of Geological Engineering, Middle East Technical University, Ankara 06531, Turkey

ARTICLE INFO

Article history:
Received 22 July 2011
Accepted in revised form 31 January 2012
Available online 3 March 2012

Keywords:
Oceanic anoxic event 1a
Oceanic red bed 1
OAE1a-ORB1 transition
Aptian
Turkey

ABSTRACT

We performed a detailed study of the stratigraphic transition from the early Aptian oceanic anoxic event 1a (OAE1a) to the oceanic red bed 1 (ORB1) along the pelagic Yenicesihlar section in the Mudurnu region of central Turkey. The Selli-equivalent level of the OAE1a (approximately 2.1 m thick) consists of black to dark-grey shales interbedded with grey marlstones with total organic carbon contents up to 2.05%. The carbon isotopic record shows a negative excursion (C3 stage, 0.58 m in thick) at the bottom of the Selli-equivalent black shales and a stepwise positive excursion (C4 to C6 stages, 1.52 m in thick) within the Selli-equivalent black shales. The OAE1a-ORB1 transitional interval (~20.3 m in thick) displays an alternation of light-grey limestones with grey marls or shales that links the anoxic environment of the Selli-equivalent black shales at the bottom and the highly oxic environment of the ORB1 at the top. The OAE1a-ORB1 transition corresponds to stable carbon isotopic C7 and C8 stages, and based on the cyclostratigraphy, the transition lasted for approximately 1.3 Myr, which is very close to the duration of the OAE1a (1.1–1.3 Myr). The $\delta^{18}O$ values in the transitional interval are variable and generally show an increase towards the ORB1, when the climate became relatively cool.

1. Introduction

The mid-Cretaceous is marked by major perturbations in the global climate, the ocean and the carbon cycle (e.g., Leckie et al., 2002; Jenkyns, 2003; Wagreich et al., 2011), as evidenced by intervals of significant, widespread environmental changes represented by geologically brief (≤1 Myr; Bralower et al., 1994) episodes known as oceanic anoxic events (OAEs) (Schlanger and Jenkyns, 1976; Jenkyns, 1980; Arthur et al., 1990; Jenkyns, 2010). The early Aptian OAE1a is a significant Cretaceous anoxic event that occurred in oceans worldwide and is characterised by a global distribution of organic-rich deposits (i.e., the Selli level; Coccioni et al., 1989; Jenkyns, 2003), extreme greenhouse conditions (e.g., Dumitrescu et al., 2006; Ando et al., 2008), increases in continental weathering and runoff (Michalík et al., 2008; Najarroa et al., 2011), a biocalcification crisis (Erba, 1994; Erba et al., 2010), and major perturbations in global carbon cycling (e.g., Menegatti et al., 1998; Weissert and Erba, 2004; Méhay et al., 2009).

The onset of the OAE1a coincides with a pronounced, short-lived negative $\delta^{13}C$ excursion in global oceanic and terrestrial isotopic carbon compositions (e.g., Menegatti et al., 1998; van Breugel et al., 2007; Millán et al., 2009). A massive release of isotopically light CO_2 from volcanic sources or by the oxidation of methane during the dissociation of marine gas hydrates has been proposed to explain this negative excursion (Jahren et al., 2001; Wagner et al., 2007; Méhay et al., 2009). The negative excursion in $\delta^{13}C$ is followed by a shift towards positive values as a result of increased organic carbon burial during the deposition of organic matter and black-shale formation (e.g., Bralower et al., 1994; Menegatti et al., 1998). It has been suggested that the OAE1a was initially triggered by increased global temperatures due to high atmospheric CO_2 levels linked to the emplacement of the large igneous provinces of the Ontong Java Plateau (e.g., Larson and Erba, 1999; Méhay et al., 2009; Tejada et al., 2009; Kuroda et al., 2011).

Most previous studies have been performed on the OAE1a black shales or on the record preceding the OAE1a (e.g., Keller et al., 2011; Kuhnt et al., 2011; Stein et al., 2011 and references therein). Less attention has been paid to the changes after the OAE1a. The Cretaceous oceanic red beds (CORBs, Hu et al., 2005) were formed in the Tethyan Ocean shortly after the OAE1a, during the late Aptian

* Corresponding author. Tel.: +86 25 8359 3002; fax: +86 25 8368 6016.
E-mail address: huxm@nju.edu.cn (X. Hu).

0195-6671/$ – see front matter © 2012 Elsevier Ltd. All rights reserved.
doi:10.1016/j.cretres.2012.01.007

(Hu et al., 2006a; Wang et al., 2011). In the Umbria–Marche basin of Italy, eight pinkish, reddish, or maroon bands and zones occur in the interval from the Selli level (OAE1a) to the Bonarelli level (OAE2), which suggests variable palaeoceanographic conditions and perhaps indirectly indicates changes in palaeoclimate (Hu et al., 2006a). Similarly, the formation of red-bed facies occurred 1.1–1.5 Myr after the latest Cenomanian Bonarelli level of OAE2, as recorded in many Tethyan marine successions (Hu et al., 2006a, 2009; Wagreich et al., 2009; Wang et al., 2011). To date, the transition and environmental changes from the black shales of the OAE1a to red-bed facies have not been well documented. In an effort to better understand the palaeoenvironmental changes during the transition from the OAE1a to the ORB1, we herein report a continuous pelagic stratigraphic succession in central Turkey (Fig. 1).

2. Geological setting

The study area is located near the town of Mudurnu in central Turkey (Fig. 1). This area is situated on the Sakarya zone of Pontides (Okay and Tuysuz, 1999), which is delimited by Tethyan suture zones including the Intra-Pontide suture zone to the north and the Izmir-Ankara-Erzincan suture zone to the south (Sengor and Yilmaz, 1981; Okay and Tuysuz, 1999). The studied stratigraphic section lies in the Mudurnu basin, in the central part of the Sakarya zone, which was situated in the southern margin along the Sakarya continent during the Cretaceous (Kocyigit et al., 1991; Gorur and Tuysuz, 2001). The Mesozoic-Cenozoic sedimentary succession over the Palaeozoic to the Triassic metamorphic basement characterises the Mudurnu basin. The Upper Jurassic to Cretaceous successions consist of pelagic shelf carbonates, cherts, and volcaniclastics and are overlain by Upper Cretaceous slope and basinal deposits (Altiner et al., 1991). Lower Cretaceous (Berriasian to late Aptian) pelagic carbonates alternating with black shales/mudstones belong to the Sogukcam Limestone (Altiner et al., 1991; Yilmaz, 2008). The overlying Albian-Santonian Yenipazar Formation is characterised by turbidites/volcano-turbidites and pelagic carbonates (Yilmaz, 2008). The boundary between the Sogukcam Limestone and the Yenipazar Formation in the Mudurnu basin is a disconformity, where the topmost layer of the Sogukcam Limestone is cut across by structures similar to 'Neptunian dykes' (Yilmaz, 2008).

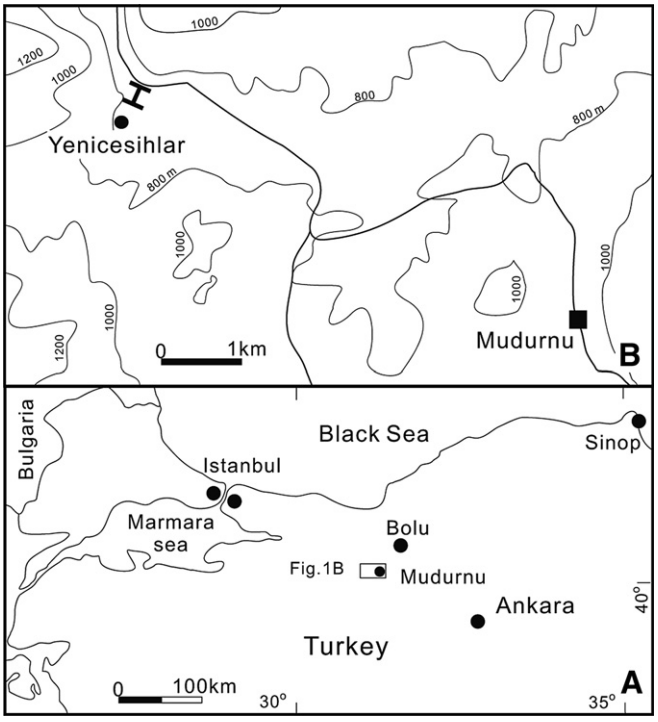

Fig. 1. A) Geographic location of the study region in Turkey; B) geographic location of the Yenicesihlar section near Mudurnu.

3. Stratigraphy and petrology

The studied Yenicesihlar section (E40°30′00.54″, N31°7′29.05″, elevation 725 m; Fig. 1B) is a sequence approximately 33 m thick within the upper part of the Sogukcam Limestone (Fig. 2A). This section was described at the centimetre scale in the field, and a total of 173 samples, at a resolution of 10–20 cm, were taken for laboratory analyses. The studied stratigraphic section of the Sogukcam Limestone can be further divided into four stratigraphic units (Fig. 2A): 1) Unit 1, 7.1 m thick, consisting of light grey to yellowish grey bioturbated limestones occasionally interbedded with thin beds of calcareous shales and marlstones; 2) Unit 2, 2.1 m thick, black or dark grey shales with grey marlstones and limestones—the black shales were within the planktonic foraminifera zone of *G. blowi* (early Aptian), and their presence was interpreted as an equivalent of the OAE1a (Yilmaz et al., 2004; Yilmaz, 2008); 3) Unit 3, approximately 20.3 m thick, displays an alternation of white to light-grey bioturbated limestones with very thinly bedded (1–5 cm) grey calcareous marls or shales—in some parts, centimetre-thick brownish grey, parallel laminated, silty limestones occur, which may be interpreted as calci-turbidites; 4) Unit 4, approximately 3.5 m thick, pinkish to light brownish limestones. The top of the measured section shows 'Neptunian dyke'-like structures and represents the boundary of the Sogukcam Limestone and the overlying Yenipazar Formation. The reddish unit 4 was assumed to be equivalent to the late Aptian oceanic red beds (ORB1) (Yilmaz, 2008) (Fig. 2C).

Microscopic analyses in thin sections and the identification of sedimentary structures in the field indicate the following facies types:

1) Wackestone/packstone: red coloured, bioturbated, bioclastic packstone with abundant bivalve (Fig. 3A) or planktonic foraminifera including glauconite and iron oxide minerals (Fig. 3B) are found at the top of the section in stratigraphic unit 4. White-beige coloured packstones/wackestones with planktonic foraminifera (Fig. 3C) or abundant radiolaria (Fig. 3D) are observed throughout the section, with an alternation of black shales and marls, and can be more clearly observed in stratigraphic unit 3. These facies carry important information in terms of understanding deposition of pelagic red beds.
2) Black shale: thicker black shale facies intervals are observed within the lower part of the measured section, and thinner facies are observed as alternating beds with limestones along the section; the best examples can be observed in stratigraphic unit 2. The black shales (Fig. 3E) are composed of organic matter, calcareous/siliceous silt, glauconite and a few pyritised radiolaria. Bioturbation is not dominantly recorded. Thin lamination can be observed in some places.
3) Marl: bluish coloured, thin-bedded marls are observed as alternating layers with thicker limestones. The marls display planktonic foraminifera as a biogenic component and some siliciclastic silt contribution. This facies can be observed in three stratigraphic units; the upper part of unit 1, the lower and upper parts of unit 2, and the lower part of unit 3.
4) Lime mudstone: white-beige coloured, medium to thick, bedded lime mudstones include planktonic foraminifera (Fig. 3F) and

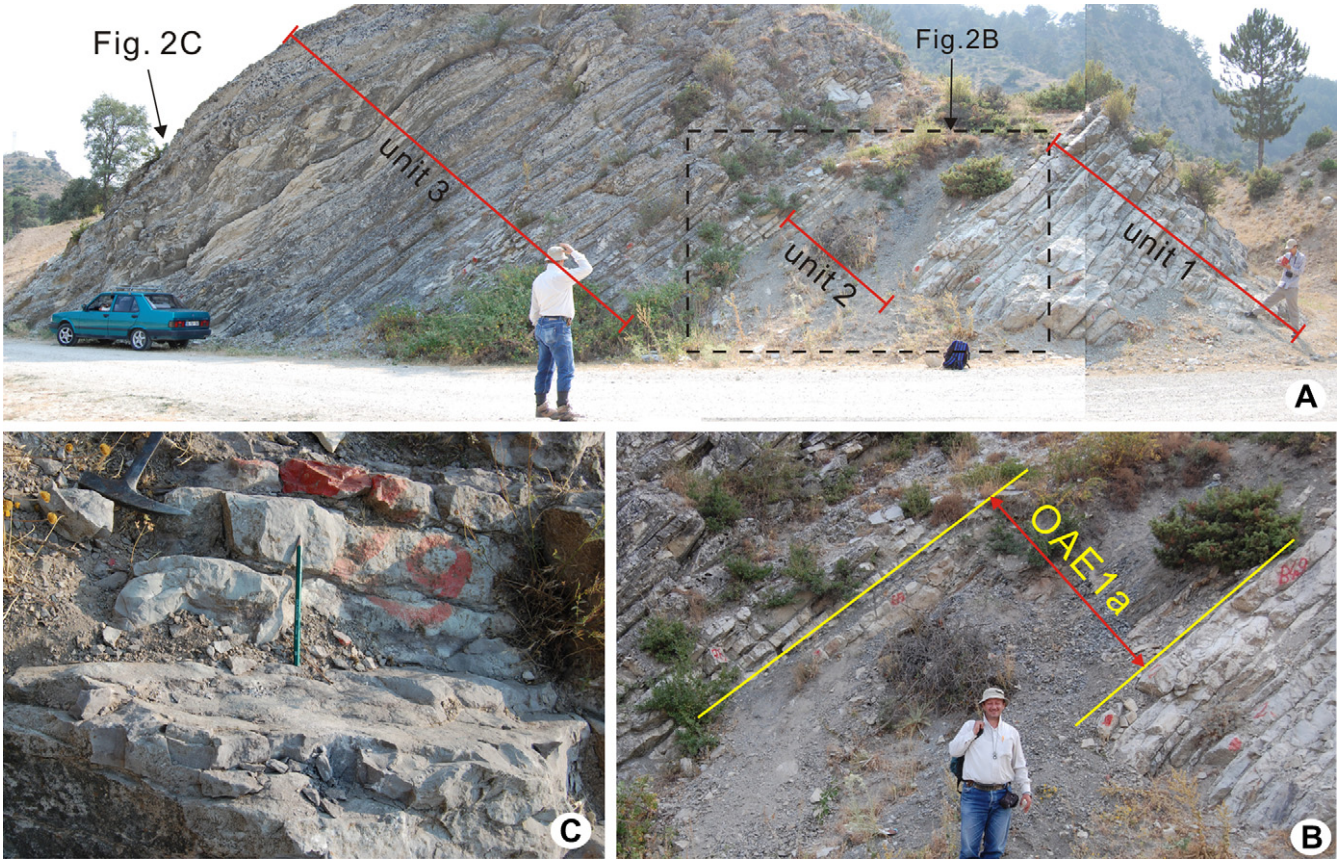

Fig. 2. Field photos in the Yenicesihlar section. A) Panoramic photograph of the Yenicesihlar section, showing the transition from the early Aptian OAE1a to the first red bed—ORB1. The positions of photographs B and C are marked. The person in the photograph (at ~1.7 m tall) provides a scale. B) close-up photograph of the early Aptian OAE1a, which is approximately 2.1 m in stratigraphic thickness; C) close-up photo of the ORB,1 showing the pinkish-red limestones. The short, red paint line above the pale reddish number represents the stratigraphic disconformity between the Sogukcam Limestone and the Yenipazar Formation. A hammer and a pencil are shown as scales. (For interpretation of the references to colour in this figure legend, the reader is referred to the web version of this article.)

sporadic radiolaria. This facies can be best observed in the lower part of stratigraphic unit 1 and upper part of unit 3.

Along the stratigraphic section, there was no record of intense diagenetic masking on the microfacies, but some calcite growths were recognised within planktonic foraminiferal chambers.

4. Analytical methods

4.1. Total organic carbon (TOC)

The TOC of 67 samples from the Yenicesihlar section was determined on the LECO CS-200 carbon-sulphur instrument at the Wuxi research institute of petroleum geology of SINOPEC, China.

4.2. Diffuse reflectance spectrophotometry (DRS)

Samples from the Yenicesihlar section were studied by the DRS method following the procedures described in Ji et al. (2002). Samples were ground to <38 μm, and spectral slides were prepared. Ground samples were suspended in distilled water to produce a slurry on glass microslides, which were then smoothed, dried slowly at low temperature (<40 °C), and analysed in a Perkin–Elmer Lambda 6 spectrophotometer with a diffuse reflectance attachment (a reflectance sphere), with scanning from 400 to 2500 nm, at the Institute of surficial geochemistry at Nanjing University. Data processing was restricted to the visible range (400–700 nm). The data are reported as percent reflectance relative to the Spectralon® standard. First-derivative values (percent per nanometre) were calculated at 10 nm intervals to enhance the variability of the reflectance data.

4.3. Spectral analyses

The studied section is dominated by centimetre- to decimetre-thick beds. Spectral analyses of bed thickness across the interval representing the transition from the OAE1a to the ORB1 were performed, using the technique of Muller and MacDonald (2000), to detect dominant sedimentary cycles. This technique involves linear interpolation of raw depth series of bed thickness, detrending, and Fast Fourier Transforms (FFTs) of the prepared series. FFTs of the prepared series were performed in the depth domain to yield a set of spectral peaks. A band-pass filter of 1/3000 to 1/10 cycles/mm was applied to remove low and high frequencies that are likely far beyond orbital frequency bands. In addition, a Monte Carlo approach was employed to estimate noise levels, in which FFTs on 1000 randomly generated datasets were combined to construct a 95% confidence curve (Mader et al., 2004). Only spectral peaks standing above the noise level are considered statistically significant cycles. Following the approach of Fischer (1991), the wavelength ratios of the identified significant cycles are compared with the periodicity ratios of the orbital cycles to determine whether the sedimentary cycles represent orbital cycles. Similar ratios in the

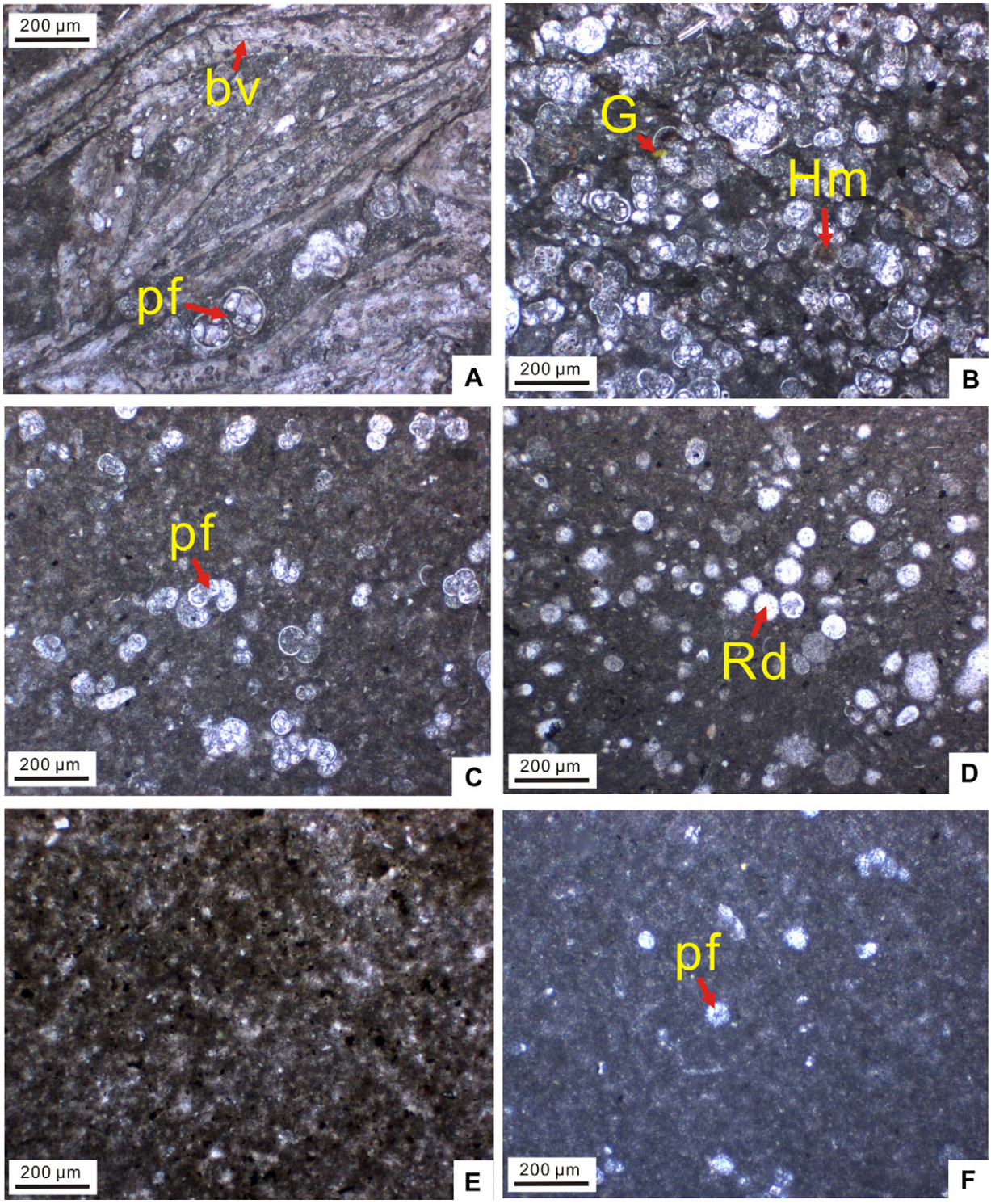

Fig. 3. Photomicrographs of microfacies in the Mudurnu section. The lengths of the scale bars are indicated in each photograph. A) red-coloured bioclastic packstone (sample MYU-1); B) red-coloured packstone with abundant planktonic foraminifera (sample MYU-2); C) wackestone with planktonic foraminifera (sample MY-131); D) packstone with abundant radiolaria (sample MY-143); E) silty black shale with iron and glauconite (sample MY-53); F) lime mudstone with planktonic foraminifera (sample: MY-2). Abbreviations: bv, bivalve shell; G, glauconite; Hm: haematite; pf, planktonic foraminifera; Rd, radiolaria.

depth and time domains and the characteristic features of their modulation patterns, such as precession by eccentricity, constitute the basis for interpreting the identified sedimentary cycles as orbital cycles. An orbital timescale can be established once orbital cycles are recognised.

4.4. Stable carbon and oxygen isotopes

The sampled lithologies include homogeneous light-grey, marly, micritic limestones without apparent late diagenetic cementation, grey, calcareous marlstones and shales. Stable carbon

and oxygen isotopic compositions of 163 whole rock samples were analysed using a Finnigan MAT Delta Plus XP mass spectrometer equipped with an automated carbonate reaction device (Gasbench II) at the State Key Laboratory for Mineral Deposits Research, Nanjing University, China. Samples were subsequently reacted with purified orthophosphoric acid at 70 °C and analysed in-line using the mass spectrometer. The data are expressed as per-mil deviations from the Peedee belemnite (PDB) standard. Duplicate measurements of the same working standards yielded identical values to within the limits of analytical precision (1σ): 0.05‰ for $\delta^{13}C$ and 0.07‰ for $\delta^{18}O$.

5. Results

5.1. Total organic carbon

The TOC values of the grey limestones from unit 1 (14 samples) are very low, at 0.02–0.03% (Fig. 4). In total, 27 samples with TOC values were taken from unit 2—the Selli-equivalent black shale (Fig. 4). The TOC values of the grey limestones are very low (0.02–0.08%, 7 samples). The dark grey shales have TOC values varying from 0.13 to 0.42% (11 samples). The black shales have high TOC values, ranging from 0.9 to 2.05% (5 samples). At the bottom of

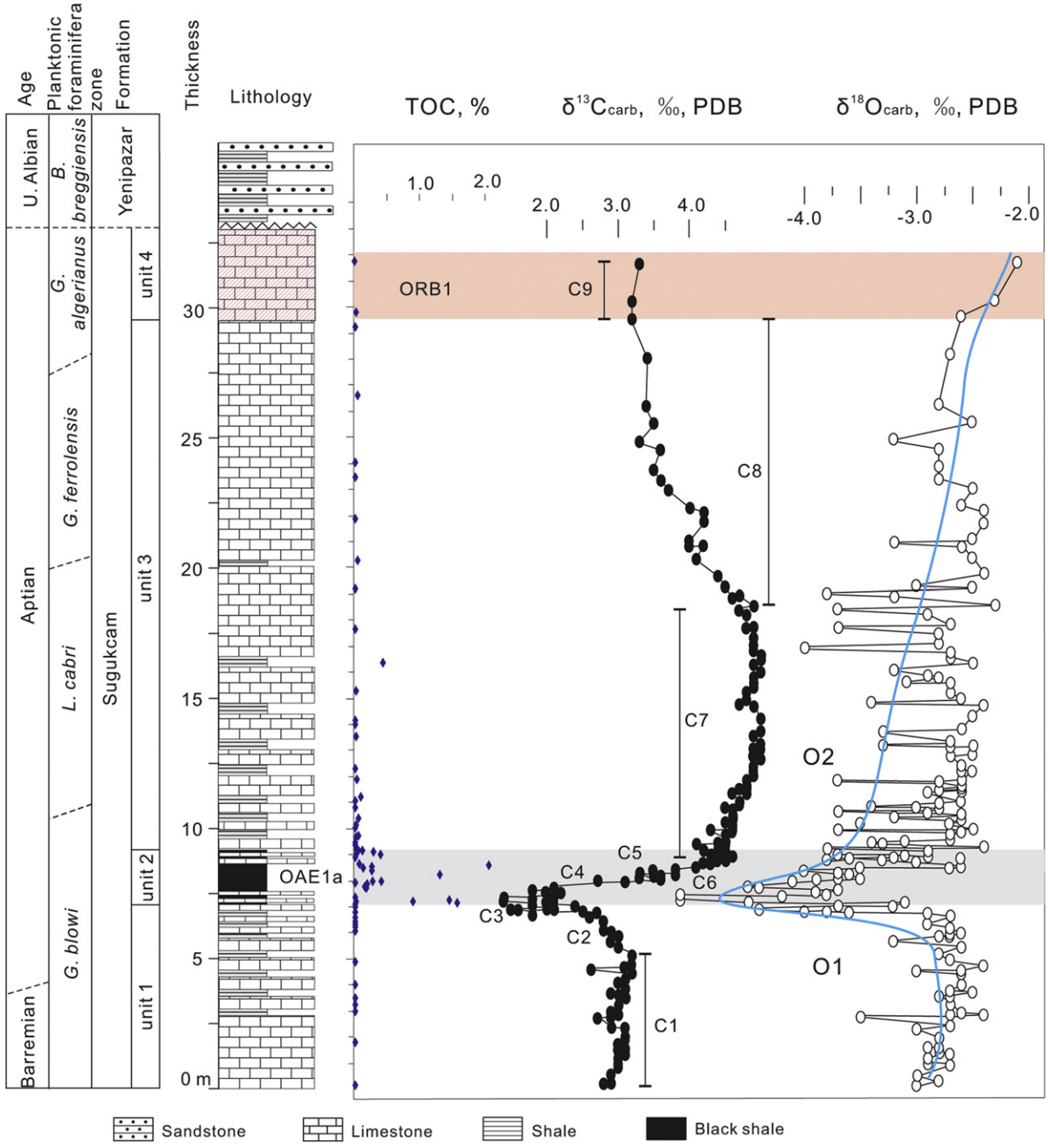

Fig. 4. Geochemical profiles of the measured Yenicesihlar stratigraphic section: TOC and stable isotopes ($\delta^{13}C$ and $\delta^{18}O$). The planktonic foraminiferal zones are taken from Yilmaz (2008). The determination of $\delta^{13}C$ and $\delta^{18}O$ stages follows Menegatti et al. (1998).

the Selli-equivalent black shale, the TOC value abruptly increases to 1.57%. The TOC values of the grey limestones from unit 3 (22 samples) are very low, at 0.02–0.07% (Fig. 4). Two grey shales have TOC values of 0.06–0.11%, and one dark grey sample has a TOC value of 0.44%. The TOC value of the grey limestone in unit 4 is 0.04%, whereas the light brownish sample has a low TOC value of 0.01% (Fig. 4).

5.2. Diffuse reflectance spectrophotometry

As documented by Deaton and Balsam (1991), haematite and goethite can easily be identified in the first-derivative curves of DRS data. Haematite is associated with a single prominent peak, at either 565 or 575 nm, and goethite has two first-derivative peaks, with the primary peak at 535 nm and a secondary peak at 435 nm (Balsam and Deaton, 1991; Deaton and Balsam, 1991; Li et al., 2011). The heights of both haematite and goethite peaks increase as the concentrations of these minerals increase (Deaton and Balsam, 1991; Li et al., 2011).

Light brownish limestones from the ORB1 (unit 4) in the Yenicesihlar section contain haematite based on the interpretation of the DRS data, which show a single prominent peak between 560 and 570 nm in the first-derivative curves (Fig. 5). The curves of the ORB1 are very similar to those of the reddish limestones in the Gubbio, Italy (Hu et al., 2009). Both the light-grey limestones and the black shales from the Yenicesihlar section lack both haematite and goethite minerals because there are no peaks corresponding to haematite or goethite in the first-derivative DRS curves (Fig. 5).

5.3. Cyclostratigraphy

Bed thickness data for the studied section are shown in Fig. 6A. To stabilise the variance of the series (Weedon, 2003), the raw thickness measurements are log-transformed (Fig. 6B). Spectral analysis of the log-transformed thickness series of the section reveals dominant cycles with wavelengths of ~ 2,226, 1,548, 559,

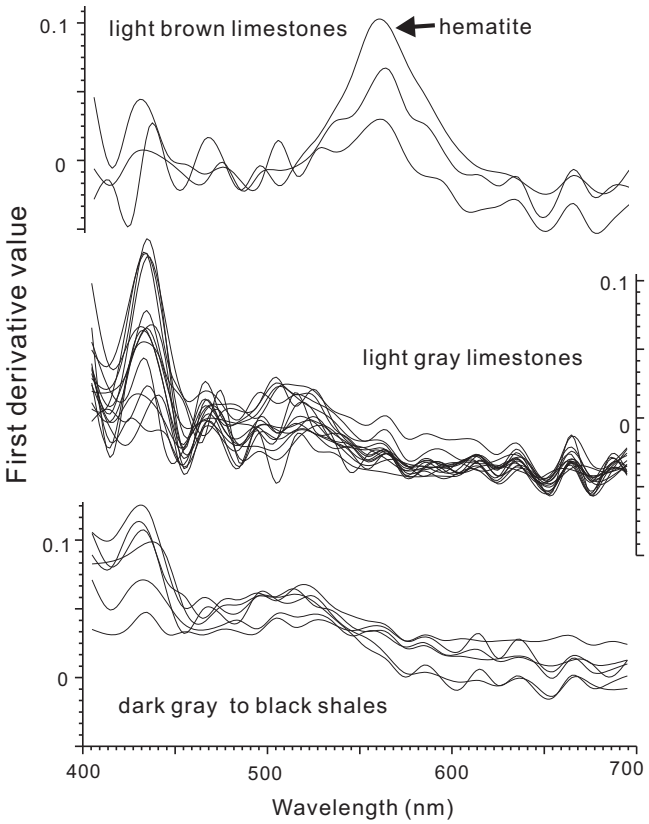

Fig. 5. First derivatives of the diffuse reflectance spectrometry (DRS) data for the light brownish limestones (upper), light grey limestones (middle) and dark grey to black shales (lower) from the Yenicesihlar section. Note the peak at ~565 nm in the light brownish limestones, which represents haematite mineral.

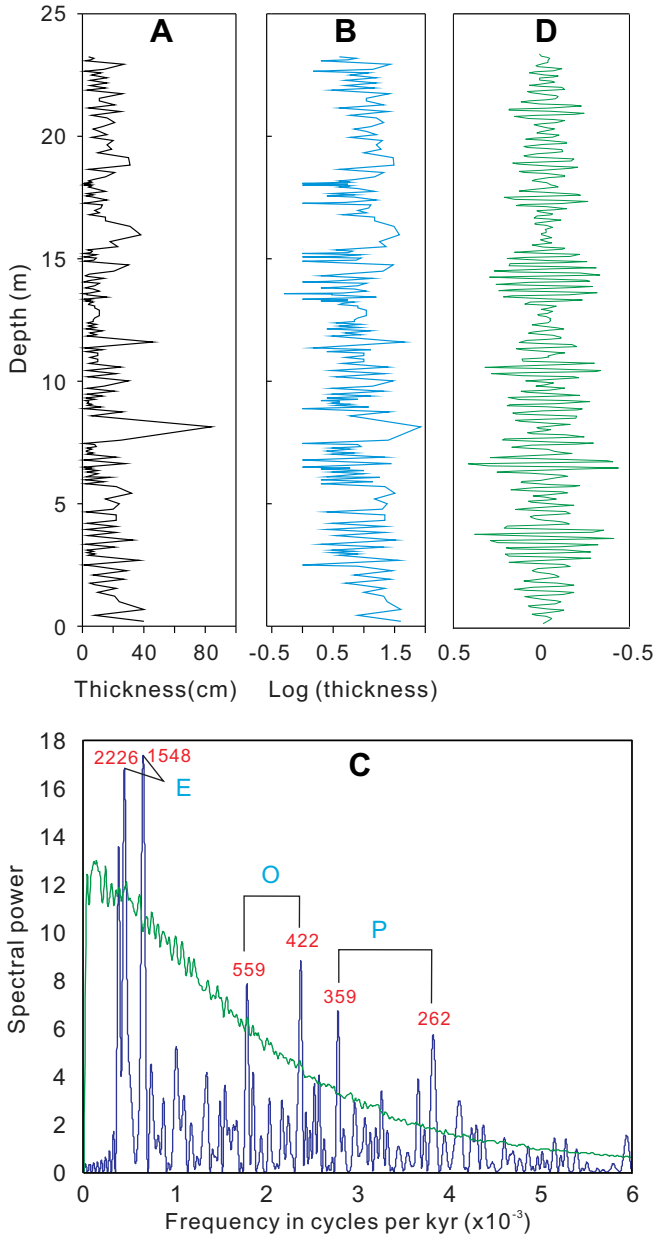

Fig. 6. Spectral analyses of bed thickness measurements. (A) bed thickness of the section; (B) log-transformed bed thickness data; (C) spectral analysis of the log-transformed bed thickness showing statistically significant sedimentary cycles that are interpreted to represent orbital cycles (see text for interpretation). Numbers above peaks are cycle wavelengths in mm. E, eccentricity; O, obliquity; P, precession; (D) a pronounced modulation pattern showing that 4 to 8 short wavelength cycles are superimposed over long wavelength cycles, representing precession and eccentricity, respectively.

422, 359, and 262 mm. It is well known that orbital cycles operate in several modes, particularly for obliquity and precession (Hinnov, 2004). For example, the obliquity has a primary mode of 41 kyr but can also have modes of 54 kyr, 39 kyr, and 29 kyr. Precession can occur at modes of 24, 22, 19, and 17 kyr. The short eccentricity displays principal modes of 95 and 125 kyr, but modes can also occur with 99 kyr and 131 kyr periodicities (Hinnov, 2004). Cycles of 559 and 262 mm yield a wavelength ratio of 2.13, which is similar to the value of 2.16 for the 41:19 kyr periodicity ratio of the obliquity and precession cycles. Cycles of 422 and 359 mm yield a wavelength ratio of 1.18, resembling the 1.208 ratio of the 29 kyr obliquity and the 24 kyr precession. Cycles of 2226 and 1548 mm exhibit a wavelength ratio of 1.438, which is comparable to the ratio of 1.316 for the 125 kyr and 95 kyr periodicities and similar to the 1.379 ratio of 131 kyr and 95 kyr orbital cycles. In essence, the 2226 and 1548 mm cycles occur in the short eccentricity frequency band and may thus represent short eccentricity cycles in the sedimentary record. Similarly, the 559 and 422 mm cycles probably represent obliquity signals, and the 359 and 262 mm cycles most likely record precession. To examine this interpretation, a band-pass filter was applied to extract the 359 and 262 mm cycles representing the precession. As shown in Fig. 6D, a striking modulation pattern appears, in which the short wavelength cycles are superimposed on the long wavelength cycles, and 4–8 short wavelength cycles are typically bundled to form a ~ 2 m cycle. This modulation pattern mimics that of the modulation of precession by eccentricity, lending strong support to the above interpretation.

5.4. Stable carbon and oxygen isotopes

All the $\delta^{13}C$ values vary from +1.4‰ to +5.0‰, and the $\delta^{18}O$ values vary from −4.6‰ to −1.6‰. A cross-plot of carbon- and oxygen-isotope values shows no significant trends and lacks a pronounced slope ($R^2 = 0.168$; Fig. 7) observed in many so-called "mixing lines" produced by the addition of variable quantities of isotopically homogeneous cement to isotopically homogeneous skeletal calcite (e.g., Marshall, 1992). This type of isotopic signature in the studied section may be considered to be a record of primary palaeoceanographic information.

The stable carbon isotopes of whole rocks can be divided into nine stages (C1–C9, Fig. 4), following the classification of Menegatti et al. (1998). The $\delta^{13}C$ values first remain stable and vary from +2.8‰ to +3.2‰ in stage C1 and then decrease slowly to the value of +2.5‰. At the bottom of the Selli-equivalent black shales, the $\delta^{13}C$ value sharply falls to +1.8‰, which marks the C2/C3 boundary. Within the C3 stage, the $\delta^{13}C$ values remain at 1.4 to +1.8‰, with one peak at +2.0‰ to +2.4‰ (Fig. 8). Subsequently, the $\delta^{13}C$ values show an abrupt step-like positive shift from +1.8‰ to +3.6‰ in C4 (Fig. 8). In the C5 stage, the $\delta^{13}C$ values remain at +3.3‰ to +3.8‰. There is a second abrupt increase from +3.8‰ to +4.6‰ in the C6 stage (Fig. 8). In the C7 stage, the $\delta^{13}C$ values remain at +4.1‰ to +5.0‰, which is regarded as a carbon isotopic plateau. Subsequently, the $\delta^{13}C$ values gradually decrease (C8) and approximate the pre-excursion level of ~3.2‰ (C9) (Fig. 4). The carbon isotopic stages C3 through C6 are closely related to the Selli-equivalent black shales (Fig. 4).

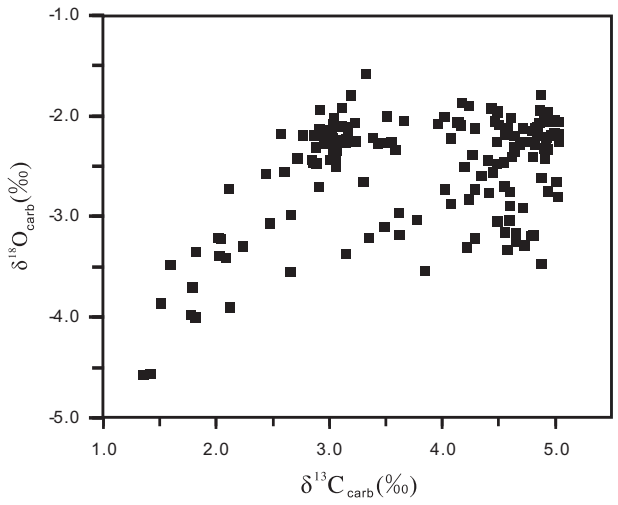

Fig. 7. Cross-plot of stable carbon and oxygen isotopes ($\delta^{13}C$ vs. $\delta^{18}O$).

The $\delta^{18}O$ profile shows oxygen isotopic variations between −4.6‰ and −1.6‰ (Fig. 4). The $\delta^{18}O$ values were −2.0 to −2.5‰ during the earliest Aptian, and shifted towards more negative values, reaching as low as −4.6‰ during the OAE1a (Fig. 8). Just 7 cm below the bottom of the Selli-equivalent black shales, the $\delta^{18}O$ values start to decrease. The $\delta^{18}O$ values within the Selli-equivalent black shales are variable and can be further divided into 4 decreasing–increasing couplets (Fig. 8). After the OAE1a, the $\delta^{18}O$ values are variable and generally show an increase towards the ORB1, where the $\delta^{18}O$ values have less negative values (−2.1 to −1.6‰, Fig. 4).

6. Discussion

6.1. Palaeoenvironmental changes from the OAE1a to the ORB1

Facies analysis along the measured stratigraphic section revealed that pelagic carbonate deposition took place around an upper slope environment before the OAE1a anoxic conditions occurred. There was no coarse siliciclastic input from terrestrial sources. Muddy carbonates were generally bioturbated, and nearly all bioturbations were filled with dark-coloured muds that were probably derived from the overlying black shales. During anoxic conditions, bioturbating organisms were not active due to low oxygen level, and organic muds with few biota were deposited. Following the anoxic conditions, carbonates with planktonic organisms covered the slope with alternations of pelagic limestones and black shales, indicating that changing environmental conditions were repeated frequently. For a certain period, carbonates display a less frequent alternation with black shales on the pelagic environment. The reddish pelagic limestones (unit 4, ORB1) are similar to the Scaglia Rossa facies in Italy. It has been well documented that the reddish limestones of the Scaglia Rossa facies in Italy were deposited in highly oxic environments, most probably due to high dissolved-oxygen content at the sediment-water interface and/or low bioproductivity (Hu et al., 2005, 2006a, 2006b, 2009; Wang et al., 2004, 2005, 2009; Cai et al., 2009). The reddish colour of the Cretaceous pelagic limestones in central Italy is due to the occurrence of iron oxides, mainly haematite (Cai et al., 2009; Hu et al., 2009), in the form of authigenic nano-grains formed in oxic conditions at the time when the red limestones were deposited (Cai et al., 2012). In unit 4 of the studied section, the reddish limestones show characteristic peaks of haematite mineral (Section 5.2), which implies an oxic environment for this stratigraphic interval.

The palaeoenvironmental changes from the OAE1a to the ORB1 in central Turkey are similar to those observed for central Italy (see Hu et al., 2006a), where the Selli-equivalent black shales are separated from the ORB1 by a grey limestone interval. This interval is approximately 2.5 m thick in the Gorgo a Cerbara section (Wang et al., 2011) and approximately 3 m thick in the Piobbico core (Erba, 1988).

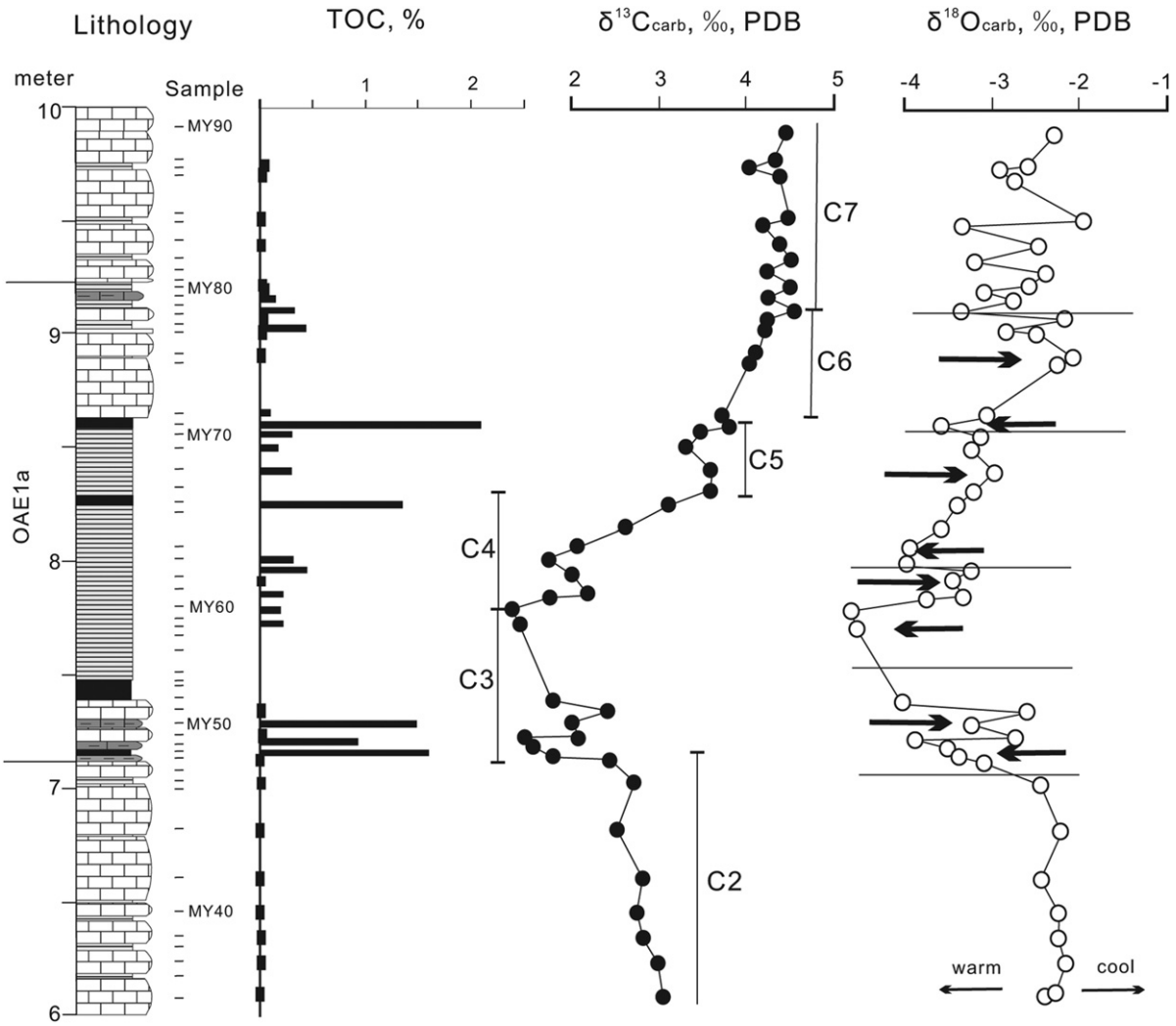

Fig. 8. Geochemical profiles of TOC and stable isotopes ($\delta^{13}C$ and $\delta^{18}O$) near the OAE1a of the Yenicesihlar section.

6.2. *Duration of the transition from the OAE1a to ORB1*

It is well known that the periodicities of obliquity and precession vary with time, and those of the eccentricity remain constant in the geologic past (Laskar et al., 2004). The periodicity of the precession was approximately 20.3 kyr at 120 Ma according to Berger and Loutre (1994). The studied section consists of cm- to dm-thick beds of limestones and marls and a condensed unit of black shales. The thickness of individual beds in depths of the section from 0 m to 23.24 m was measured, except for the black shale unit, where laminae and/or very thin beds were grouped during measurements. Spectral analysis of the thickness of the measured section reveals dominant sedimentary cycles that are tentatively interpreted as orbital cycles (section 5.3). The isolated cycles representing precession display a modulation pattern in which precession is modulated by short eccentricity (Fig. 6D). Both cycles representing precession and short eccentricity can be used to estimate their durations. Because the black shale unit is highly condensed and because laminae and/or very thin beds were grouped, it is not possible to use these cycles to estimate durations for the black shales.

The transition from the OAE1a to the ORB1 is defined from 9.22 m to 29.56 m in the section and corresponds to carbon isotope stages C7 and C8 in the chemostratigraphy (Fig. 4). The lower part (9.22–23.24 m) of the transition interval contains approximately 47 precession cycles, corresponding to ~ 950 kyr, or 8.5 short eccentricity cycles, corresponding to ~ 850 kyr. Therefore, the lower part (9.22 m–23.24 m) of the transitional interval represents ~ 900 kyr on average. The mean sedimentation rate of the stage is calculated as ~1.56 cm/kyr. The mean sedimentation rates of the strata adjacent to the OAE1a interval in a pelagic setting of the Cismon section and in a hemipelagic depositional environment of the Santa Rosa section are estimated to be nearly 1.0 cm/kyr and ~ 2.1 cm/kyr, respectively (Li et al., 2008). The estimated 1.56 cm/kyr sedimentation rate for the pelagic setting of the Yenicesihlar section is thus compatible with the sedimentation rates at Cismon (Italy) and Santa Rosa (Mexico), which may provide additional support for the interpretation that the dominant sedimentary cycles represent orbital variations. Assuming that these cycles persist throughout the rest of the section, the upper part (23.24 m–29.56 m) of the transitional interval would represent ~400 kyr. Thus, the duration of the transition from the OAE1a to the ORB1 would be ~ 1.3 Myr. The transitional interval from the top of the Selli-equivalent black shales to the bottom of the ORB1 corresponds to the carbon isotopic stages C7 and C8 (Fig. 4). The C7 stage contains ~ 34 precession cycles, corresponding to ~ 690 kyr, or ~ 6 short eccentricity cycles, corresponding to ~ 600 kyr. Thus, the C7 stage persisted for ~ 650 kyr. Because the transition from

OAE1a to ORB1 that contains carbon isotope stages C7 and C8 occurred over 1.3 Myr, as estimated above, the negative shift of the C8 stage thus lasted for ~ 650 kyr. It is interesting to note that the duration of OAE1a (C3 to C6 stages) has been estimated at approximately 1.11 Myr (Malinverno et al., 2010) or 1.27 Myr (Li et al., 2008), which is very close to the ~ 1.3 Myr duration of the OAE1a-ORB1 transitional interval reported herein. This concordance appears to suggest that, from the carbon isotope perspective, the system requires similar amounts of time for recovery (i.e., passage from stage C7 to C8) to that of the perturbation associated with the OAE1a (stages C3 to C6), although detailed recovery dynamics remain elusive.

6.3. Carbon isotopes and the OAE1a-ORB1 transition

The carbon isotopic record from the bottom of the OAE1a to the bottom of the ORB1 shows four distinct stages: 1) a negative excursion (C3, 0.58 m); 2) a positive excursion (C4 to C6, 1.52 m); 3) an isotopic plateau (C7, 9.48 m); and 4) an isotopic decrease (C8, 10.86 m) (Fig. 4).

It has been documented for a long time that the OAE1a is characterised by a pronounced negative carbon isotope excursion preceding the $\delta^{13}C$ increase (e.g., Menegatti et al., 1998; Bellanca et al., 2002; Herrle et al., 2004; Ando et al., 2008; Kuhnt et al., 2011; Fig. 9). Putative processes supplying isotopically light carbon at the onset of the OAE1a include large-scale volcanogenic carbon dioxide emission and/or the dissociation of gas hydrates and/or thermal metamorphism of coals, either singly or in combination (e.g., Erba, 1994; Larson and Erba, 1999; Jahren et al., 2001; Tejada et al., 2009; Kuhnt et al., 2011). A crucial point in this debate is the duration of the negative $\delta^{13}C$ excursion because volcanic CO_2 ($\delta^{13}C$: −5‰ to −7‰) would need to be released over a longer time span to produce the same isotopic effect as a short-lived CH_4 release ($\delta^{13}C$: −60‰) (Wagner et al., 2007; Méhay et al., 2009). Previous studies suggested that the main negative carbon isotopic shift of the OAE1a begins at the lowest stratigraphic levels of the organic-rich black shale, at the level where TOC values start to rise (Menegatti et al., 1998; Jenkyns, 2010). However, our new high-resolution carbon isotope records from Turkey indicate that the negative carbon isotopes remain for 58 cm, which would last for 0.32 kyr if we take 1.2 Ma (Li et al., 2008; Malinverno et al., 2010) as the mean duration of the OAE1a (Table 1). Our data are in agreement with the data for France reported by Kuhnt et al. (2011), where the C3 stage lasted >100 ka. The long duration and relatively low amplitude (0.7‰) of the negative $\delta^{13}C$ excursion favours the hypothesis that enhanced volcanic CO_2 emission and/or pulsed methane dissociation were instrumental in triggering the OAE1a, as previously suggested by other authors (Erba, 1994; Larson and Erba, 1999; Tejada et al., 2009). It should be noted that the amplitude of the negative $\delta^{13}C$ excursion in the Mudurnu is similar to those from the Cismon in Italy (Menegatti et al., 1998), Sicilyin SW Italy (Bellanca et al., 2002) and SE France (Herrle et al., 2004; Kuhnt et al., 2011) but smaller than that from the Deep Sea Drilling Project (DSDP) site 463 in the Pacific Ocean (Ando et al., 2008; Fig. 9).

The positive carbon isotope shift at the onset of the OAE1a has previously been regarded as abrupt (Menegatti et al., 1998) or continuous (Li et al., 2008). As shown in Fig. 8, the record in the Mudurnu shows a subsequent shift towards more positive values

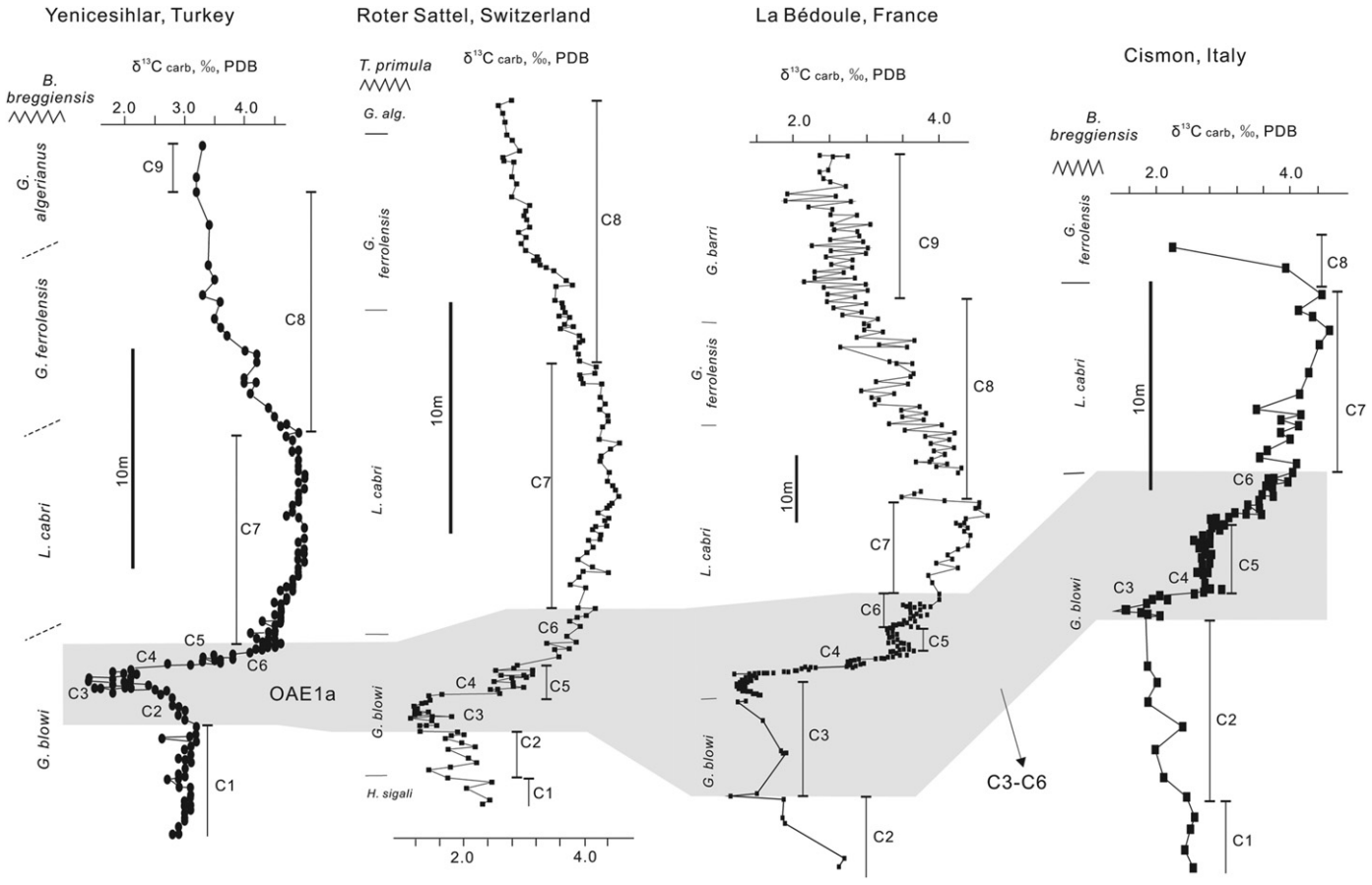

Fig. 9. Aptian chemostratigraphic correlation of stable carbon isotopes from the Yenicesihlar section (this study, central Turkey) with those of the Roter Sattel section, Switzerland (Menegatti et al., 1998), the La Bédoule, France (Kuhnt et al., 2011) and the Cismon section, Italy (Menegatti et al., 1998).

Table 1
Summaries of stratigraphic positions, thicknesses and estimated durations of the OAE1a, the ORB1, and selected intervals.

Stage	Stratigraphic position (m)	Thickness (m)	Duration (myr)	Sedimentation rate (m/myr)
ORB1	29.56–32.96	3.4	–	–
OAE1a-ORB1 transitional interval	9.22–29.56	20.34	~1.3	15.6
OAE1a	7.12–9.22	2.1	1.1 to 1.3[a]	1.7–1.9
C9	29.56–32.96	3.4	–	–
C8	18.70–29.56	10.86	0.65	16.7
C7	9.22–18.70	9.48	0.65	14.6
C6	8.70–9.22	0.52	0.29	1.8[b]
C5	8.30–8.70	0.4	0.22	
C4	7.70–8.30	0.6	0.33	
C3	7.12–7.70	0.58	0.32	
C2	5.59–7.12	1.53	–	–
C1	0–5.59	5.59	–	–

[a] Li et al. (2008) and Malinverno et al. (2010).
[b] Taken 1.2 Ma as the mean duration of the OAE1a.

(C4-C5-C6), reaching the peak values of the early Aptian $\delta^{13}C$-positive excursion (C7). The increase in the $\delta^{13}C$ values in stages C4 (from +1.4‰ to +3.6‰) and C6 (from +3.8‰ to +4.6‰) occurs at stratigraphic thicknesses of 60 cm and 52 cm, respectively (Fig. 8). If we take 1.2 Ma (Li et al., 2008; Malinverno et al., 2010) as the mean duration of the OAE1a, then the C4 and C6 stages would last for approximately 0.33 kyr and 0.29 kyr, respectively. The stepwise positive shift may have been caused by periodic increases in organic carbon burial in the black shales during the OAE1a (Berger and Vincent, 1986; Menegatti et al., 1998; Kuhnt et al., 2011).

The $\delta^{13}C$ values remain at a high plateau (C7) in a stratigraphic interval of 9.46 m (Fig. 4), which lasts for 650 kyr (section 6.2). The duration of the steadily high $\delta^{13}C$ values implies that mass and isotopic steady-state conditions were established. Assuming a gradually decreasing primary productivity during the deposition of the C7 stage, the extraction of ^{12}C into the sedimentary carbon sink would be balanced by the gradually decreasing flux of isotopically light carbon into the surface water reservoir.

Subsequently, the $\delta^{13}C$ values gradually decreased (stage C8) and approximated the pre-excursion level of ~3.2‰ (stage C9) (Fig. 9). The gradual decrease in $\delta^{13}C$ from +4.9‰ to +3.2‰ occurs in thickness of 10.86 m, corresponding to a duration of ~650 kyr (section 6.2). This long duration does not support an abrupt response for the carbon isotopic decrease. Instead, gradually diminishing organic carbon burial could have resulted in a gradual decrease in $\delta^{13}C$ values. Enhanced amounts of organic carbon and pyrite burial during the OAE1a would have resulted in a large decrease in atmospheric CO_2 concentration (Arthur et al., 1988), inducing significant global climatic cooling. Global cooling would have enhanced formation of the cold deep water, increasing its oxidising capacity due to the greater content of dissolved oxygen (Wang et al., 2011). Such an increase in the oxidising capacity of deep oceanic water would reduce the burial of organic carbon and promote the formation of oceanic red beds.

6.4. Oxygen isotopes as climate indicators?

The approximation of palaeoclimatic conditions constitutes an important tool to discriminate the palaeoenvironmental changes from the OAE1a to the ORB1. However, post-depositional processes may have altered the original geochemical signal of the rock record, and it is thus essential to assess the diagenetic state of the sedimentary succession before making any palaeoenvironmental interpretation. First, the oxygen-isotope composition of the Yenicesihlar section is characterised by slightly negative values and a lack of correlation with the $\delta^{13}C$ record ($R^2 = 0.168$ for the whole section in the Fig. 7; $R^2 = 0.345$ for the 6–10 interval on the Fig. 8). The relatively low oxygen-isotope ratios, which depart from the typical values found in poorly consolidated Cretaceous pelagic sediments (Jenkyns et al., 1994; Clarke and Jenkyns, 1999), necessarily imply a considerable diagenetic overprint. However, an overall pattern of increasingly lower $\delta^{18}O$ values with depth caused by burial diagenesis is not presented in the Yenicesihlar section. Second, the relatively good correlation between the $\delta^{18}O$ record of the Yenicesihlar section with the $\delta^{18}O$ records of the Cismon in Italy (Menegatti et al., 1998), the Gorgo a Cerbara in Italy (Stein et al., 2011) and DSDP 453 in the Pacific Ocean (Ando et al., 2008) suggests that the characteristic form of this oxygen-isotopic curve reflects primary seawater values, with any diagenetic effects similarly affecting the section in a generally consistent manner. Consequently, we refrain from inferring the palaeotemperature from these isotopic data and only consider the long-term trends.

Just 7 cm below the bottom of the Selli-equivalent black shales, the $\delta^{18}O$ values start to decrease (Fig. 8), probably indicating a warming event. A similar trend towards higher temperatures around the onset of the OAE1a followed by a cooling phase is observed in the whole-rock and belemnite records of the Vocontian Basin, in southeastern France (Godet et al., 2006; Bodin et al., 2009), and the $\delta^{18}O$ record of the Gorgo a Cerbara (Italy) (Stein et al., 2011). This significant rise in the $\delta^{18}O$ record was found just below the OAE1a at DSDP Site 463 (in the central Pacific Ocean), which corresponds to a temperature increase of 8 °C according to Ando et al. (2008).

The $\delta^{18}O$ values within the Selli-equivalent black shales are variable and can be further divided into four decreasing–increasing couplets (Fig. 8), which probably represent warm–cool climate cycles. Using the TEX86 palaeothermometer, Dumitrescu et al. (2006) reported that sea-surface temperatures during the OAE1a at Shatsky Rise in the tropical Pacific were high, ranging from 30 to 36 °C, and include two prominent cooling episodes of 4 °C. Kuhnt et al. (2011) also reported transient climate cooling during the initial $\delta^{13}C$ increase within the OAE1a in southeastern France.

After the OAE1a, the $\delta^{18}O$ values are variable and generally show an increase towards the ORB1, where the $\delta^{18}O$ values reach the highest values, which may represent the coolest climate in the late Aptian. The late Aptian is, in fact, considered to be one of the cold snaps during the greenhouse Cretaceous. Direct evidence for late Aptian global cooling is indicated by occurrences of glendonites and ice-rafted debris in Canada and in southeastern Australia (Frakes et al., 1995). Isotopic evidence for a cool late Aptian includes data from south temperate belemnites, glendonites and carbon isotopes (Weissert and Lini, 1991). A recent study reported that late Aptian global cooling is suggested by a decline of Tethyan taxa of calcareous nannofossil assemblages and a subsequent biogeographic expansion of species of high latitudinal affinities (Mutterlose et al., 2009).

7. Conclusions

The Yenicesihlar section documents the stratigraphic and palaeoenvironmental changes from the OAE1a to the ORB1 during the Aptian.

1) The OAE1a interval is approximately 2.1 m thick and consists of black to dark grey shales with grey marlstones. The black shales have high contents of organic matter, with TOC values up to 2.05%. The OAE1a-ORB1 transitional interval (~20.3 m thick) displays an alternation of light grey limestones with very thin-bedded grey marls or shales. The ORB1 (approximately 3.5 m thick) consists of pinkish to light brownish limestones.

2) The redox conditions changed from anoxic in the OAE1a black shales to oxic in the transitional interval and finally to a highly oxic environment in the ORB1 interval. The high organic carbon content and pyritisation within the black shales of the OAE1a indicated an anoxic environment. The ORB1 represents a highly oxic environment, as haematites were determined from the reddish limestones in the DRS curves.

3) The carbon isotopic record shows several perturbations in the OAE1a-ORB1 transitional interval including a negative excursion (C3, 0.58 m) in the lower part of the Selli-equivalent black shales, a stepwise positive excursion (C4 to C6, 1.52 m) within the Selli-equivalent black shales, a positive carbon isotopic plateau (C7, 9.48 m) in the lower part of the transitional interval, and a carbon isotopic decrease in the upper part of the transitional interval (C8, 10.86 m). The long duration and relatively low amplitude (0.7‰) of the negative $\delta^{13}C$ excursion (C3) in Turkey favours the hypothesis that enhanced volcanic CO_2 emission and/or pulsed methane dissociation were instrumental in triggering the OAE1a. The stepwise positive shift (C4-C5-C6 stages) may have been caused by periodic increases in organic carbon burial in the black shales.

4) The OAE1a to ORB1 transition interval corresponds to carbon isotope stages C7 and C8, which lasted for approximately 1.3 Myr. This duration is very close to the duration of the OAE1a (1.1–1.3 Myr). The C7 stage of positive carbon isotopic plateau persisted for ~ 650 kyr, and the negative carbon isotopic shift of the C8 stage also lasted for ~ 650 kyr. The C7 stage, with steadily high $\delta^{13}C$ values, implies that mass and isotopic steady-state conditions were established. The gradual decrease in $\delta^{13}C$ in stage C8 may have resulted in the reduced burial of organic carbon because a highly oxic environment prevailed.

5) A significant rise in the $\delta^{18}O$ record was found just below the Selli-equivalent black shales, likely indicating a warming event. The $\delta^{18}O$ values within the Selli-equivalent black shales are variable and can be further divided into four decreasing–increasing couplets (Fig. 8), which probably represent warm–cool climate cycles. After the OAE1a, the $\delta^{18}O$ values are variable and generally show an increase towards the ORB1. The ORB1, with high $\delta^{18}O$ values, may have formed in a time of cool climatic conditions during the late Aptian.

The transition interval from the OAE1a to ORB1 is consistent with changes in the climate and isotope record and is the key to understanding the carbon cycles related to the Cretaceous oceanic anoxic events and the Cretaceous oceanic red beds.

Acknowledgements

We thank Hehe Jiang, Gaoyuan Sun and Xiang Li for their help with the laboratory work. We thank Mr. Orhan Karaman for his help in the field. Reviewers Dr. Harilaos Tsikos and one anonymous reviewer and guest editor M. Wagreich are gratefully acknowledged for their stimulating and constructively comments. This study was financially supported by the MOST 973 Project (2011CB822001; 2006CB701402). This paper is a contribution to the IGCP555.

Appendix. Supplementary material

Supplementary data related to this article can be found online at doi:10.1016/j.cretres.2012.01.007.

References

Altiner, D., Kocyigit, A., Farinacci, A., Nicosia, U., Conti, M.A., 1991. Jurassic–Lower Cretaceous stratigraphy and palaeogeographic evolution of the southern part of North-Western Anatolia (Turkey). Geologica Romana 27, 13–81.

Ando, A., Kaiho, K., Kawahata, H., Kakegawa, T., 2008. Timing and magnitude of early Aptian extreme warming: unraveling primary $\delta^{18}O$ variation in indurated pelagic carbonates at Deep Sea Drilling Project Site 463, central Pacific Ocean. Palaeogeography, Palaeoclimatology, Palaeoecology 260, 463–476.

Arthur, M.A., Brumsack, H.J., Jenkyns, H.C., Schlanger, S.O., 1990. Stratigraphy, geochemistry and paleoceanography of organic carbon-rich Cretaceous sequences. In: Ginsburg, R.N., Beaudoin, B. (Eds.), Cretaceous Resources, Events and Rhythms-background and Plans for Research. Kluwer Academic Publications, Dordrecht, pp. 75–119.

Arthur, M.A., Dean, W.E., Pratt, L.M., 1988. Geochemical and climatic effects of increased marine organic carbon burial at the Cenomanian-Turonian boundary. Nature 335, 714–717.

Balsam, W.L., Deaton, B.C., 1991. Sediment dispersal in the Atlantic Ocean: evaluation by visible light spectra. Reviews in Aquatic Sciences 4, 411–447.

Bellanca, A., Erba, E., Neri, R., Premoli Silica, I., Sprovieri, M., Tremolaca, F., Verga, D., 2002. Palaeoceanographic significance of the Tethyan 'Livello Selli' (early Aptian) from the Hybla Formation, northwestern Sicily: biostratigraphy and high-resolution chemostratigraphic records. Palaeogeography, Palaeoclimatology, Palaeoecology 185, 175–196.

Berger, A., Loutre, M.F., 1994. Astronomical forcing through geologic time. In: de Boer, P.L., Smith, D.G. (Eds.), Orbital Forcing and Cyclic Sequences. International Association of Sedimentologists Special Publication 19, pp. 15–24.

Berger, W.H., Vincent, E., 1986. Deep sea carbonates: reading the carbon isotope signal. Geologische Rundschau 75, 249–269.

Bodin, S., Fiet, N., Godet, A., Matera, V., Westermann, S., Clément, A., Janssen, N.M.M., Stille, P., Föllmi, K.B., 2009. Early Cretaceous (late Berriasian to early Aptian) palaeoceanographic change along the northwestern Tethyan margin (Vocontian Trough, southeastern France): $\delta^{13}C$, $\delta^{18}O$ and Sr-isotope belemnite and whole-rock records. Cretaceous Research 30, 1247–1262.

Bralower, T.J., Arthur, M.A., Leckie, R.M., Sliter, W.V., Allard, D., Schlanger, S.O., 1994. Timing and paleoceanography of oceanic dysoxia/anoxia in the late Barremian to early Aptian (Early Cretaceous). Palaios 9, 335–369.

Cai, Y.F., Li, X., Hu, X.M., Chen, X.M., Pan, Y.G., 2009. Paleoclimatic approach to the origin of the coloring of Turonian pelagic limestones from the Vispi Quarry section (Cretaceous, central Italy). Cretaceous Research 30 (5), 1205–1216.

Cai, Y.F., Hu, X.X., Li, X., Pan, Y., 2012. Origin of the red colour in a red limestone from the Vispi Quarry section (central Italy): a high-resolution transmission electron microscopy analysis. Cretaceous Research 38, 97–102.

Clarke, L.J., Jenkyns, H.C., 1999. New oxygen-isotope evidence for long-term Cretaceous climatic change in the Southern Hemisphere. Geology 27, 699–702.

Coccioni, R., Franchi, R., Nesci, O., Wezel, F.-C., Battistini, F., Pallecchi, P., 1989. Stratigraphy and mineralogy of the Selli Level (early Aptian) at the base of the Marne a Fucoidi in the Umbria-Marche Apennines (Italy). In: Wiedmann, J. (Ed.), Cretaceous of the Western Tethys. Proceedings of the 3rd International Cretaceous Symposium, Tübingen, pp. 563–584.

Deaton, B.C., Balsam, W.L., 1991. Visible spectroscopy—a rapid method for determining hematite and goethite concentration in geological materials. Journal of Sedimentary Petrology 61, 628–632.

Dumitrescu, M., Brassell, S.C., Schouten, S., Hopmans, E.C., Damsté, J.S.S., 2006. Instability in tropical Pacific sea-surface temperatures during the early Aptian. Geology 34, 833–836.

Erba, E., 1988. Aptian–Albian calcareous nannofossil biostratigraphy of the Scisti a Fucoidi cored at Piobbico (central Italy). Rivista Italiana di Paleontologia e Stratigrafia 94, 249–284.

Erba, E., 1994. Nannofossils and superplumes: the early Aptian nannoconid crisis. Paleoceanography 9, 483–501.

Erba, E., Bottini, C., Weissert, H., Keller, C.E., 2010. Calcareous nannoplankton response to surface-water acidification around Oceanic Anoxic Event 1a. Science 329, 428–432.

Fischer, A.G., 1991. Orbital cyclicity in Mesozoic strata. In: Einsele, G., Ricken, W., Seilacher, A. (Eds.), Cycles and Events in Stratigraphy. Springer-Verlag, Berlin, pp. 48–62.

Frakes, L., Alley, N., Deynoux, M., 1995. Early Cretaceous ice rafting and climate zonation in Australia. International Geology Review 37, 567–583.

Godet, A., Bodin, S., Föllmi, K.B., Vermeulen, J., Gardin, S., Fiet, N., Adatte, T., Berner, Z., Stüben, D., van de Schootbrugge, B., 2006. Evolution of the marine stable carbonisotope record during the Early Cretaceous: a focus on the late Hauterivian and Barremian in the Tethyan realm. Earth and Planetary Sciences Letters 242, 254–271.

Gorur, N., Tuysuz, O., 2001. Cretaceous to Miocene palaeogeographic evolution of Turkey: implications for hydrocarbon potential. Journal of Petroleum Geology 24 (2), 119–146.

Herrle, J.O., Kößler, P., Friedrich, O., Erlenkeuser, H., Hemleben, C., 2004. High-resolution carbon isotope records of the Aptian to Lower Albian from SE France and the Mazagan Plateau (DSDP Site 545): a stratigraphic tool for paleoceanographic and paleobiologic reconstruction. Earth and Planetary Science Letters 218 (1–2), 149–161.

Hinnov, L.A., 2004. Earth's orbital parameters and cycle stratigraphy. In: Gradstein, F.M., Ogg, J.G., Smith, A.G. (Eds.), A Geologic Time Scale 2004. Cambridge Univ. Press, Cambridge, U.K., pp. 55–62.

Hu, X., Jansa, L., Wang, C., Sarti, M., BaK, K., Wagreich, M., Michalik, J., Sotak, J., 2005. Upper Cretaceous oceanic red beds (CORBs) in the Tethys: occurrences, lithofacies, age, and environments. Cretaceous Research 26, 3–20.

Hu, X.M., Jansa, L., Sarti, M., 2006a. Mid-Cretaceous oceanic red bed in the Umbria–Marche Basin, central Italy: Constraints on paleoceanography and paleoclimate. Palaeogeography, Palaeoclimatology, Palaeoecology 233, 163–186.

Hu, X., Wang, C., Li, X., Jansa, J., 2006b. Upper Cretaceous Oceanic Red Beds in southern Tibet: lithofacies, environments and colour origin. Science in China Series D-Earth Sciences 49, 785–795.

Hu, X.M., Cheng, W.B., Ji, J.F., 2009. Origin of Cretaceous oceanic red beds from the Vispi Quarry section, central Italy: visible reflectance and inorganic geochemistry. In: Hu, X.M., Wang, C.S., Scott, R.W., Wagreich, M., Jansa, L. (Eds.), Cretaceous Oceanic Red Beds: Stratigraphy, Composition, Origins and Paleoceanographic and Paleoclimatic Significance. SEPM Special Publication 91, pp. 183–197.

Jahren, A.H., Arens, N.C., Sarmiento, G., Guerrero, J., Amundson, R., 2001. Terrestrial record of methane hydrate dissociation in the Early Cretaceous. Geology 29, 159–162.

Jenkyns, H.C., 1980. Cretaceous anoxic events: from continents to oceans. Journal of the Geological Society of London 137, 171–188.

Jenkyns, H.C., 2003. Evidence for rapid climate change in the Mesozoic–Palaeogene greenhouse world. Philosophical Transactions of the Royal Society of London Series A 361, 1885–1961.

Jenkyns, H.C., 2010. Geochemsitry of oceanic anoxic events. Geochemistry Geophysics Geosystems 11(Q03004). doi:10.1029/2009GC002788.

Jenkyns, H.C., Gale, A.S., Corfield, R.M., 1994. Carbon-isotope and oxygen-isotope stratigraphy of the English Chalk and Italian Scaglia and its palaeoclimatic significance. Geological Magazine 131, 1–34.

Ji, J.F., Balsam, W.L., Chen, J., Liu, L.W., 2002. Rapid and quantitative measurement of hematite and goethite in the Chinese loess-paleosol sequence by diffuse reflectance spectroscopy. Clays and Clay Minerals 50, 208–216.

Keller, C.E., Hochuli, P.A., Weissert, H., Bernasconi, S.M., Giorgioni, M., Garcia, T.I., 2011. A volcanically induced climate warming and floral change preceded the onset of OAE1a (Early Cretaceous). Palaeogeography Palaeoclimatology Palaeoecology 305, 43–49.

Kocyigit, A., Altiner, D., Farinacci, A., Nicosia, U., Conti, M.A., 1991. Late Triassic–Aptian evolution of the Sakarya divergent margin: implications for the opening history of the Northern Neo-Tethys, in the North-Western Anatolia, Turkey. Geologica Romana 27, 81–101.

Kuhnt, W., Holbourn, A., Moullade, M., 2011. Transient global cooling at the onset of early Aptian oceanic anoxic event (OAE) 1a. Geology 39 (4), 323–326.

Kuroda, J., Tanimizu, M., Hori, R.S., Suzuki, K., Ogawa, N.O., Tejada, M.L.G., Coffin, M.F., Coccioni, R., Erba, E., Ohkouchi, N., 2011. Lead isotopic record of Barremian–Aptian marine sediments: Implications for large igneous provinces and the Aptian climatic crisis. Earth and Planetary Science Letters 307, 126–134.

Larson, R.L., Erba, E., 1999. Onset of the Mid-Cretaceous greenhouse in the Barremian–Aptian: igneous events and the biological, sedimentary and geochemical responses. Paleoceanography 14, 663–678.

Laskar, J., Robutel, P., Joutel, F., Gastineau, M., Correia, A.C.M., Levrard, B., 2004. A long term numerical solution for the insolation quantities of the Earth. Astronomy and Astrophysics 428, 261–285.

Leckie, R.M., Bralower, T.J., Cashman, R., 2002. Oceanic anoxic events and plankton evolution: biotic response to tectonic forcing during the mid-Cretaceous. Paleoceanography 17, 1–29.

Li, X., Hu, X.M., Cai, Y.F., Han, Z.Y., 2011. Quantitative analysis of iron oxide concentrations within Aptian-Albian cyclic oceanic red beds in ODP Hole 1049C, North Atlantic. Sedimentary Geology 235, 91–99.

Li, Y.X., Bralower, T.J., Montañez, I.P., Osleger, D.A., Arthur, M.A., Bice, D.M., Herbert, T.D., Erba, E., Premoli Silva, I., 2008. Toward an orbital chronology for the early Aptian Oceanic Anoxic Event (OAE1a, 120 Ma). Earth and Planetary Science Letters 271, 88–100.

Mader, D., Cleaveland, L., Bice, D., Montanari, A., Koeberl, C., 2004. High-resolution cyclostratigraphic analysis of multiple climate proxies from a short Langhian pelagic succession in the Conero Riveiera, Ancona (Italy). Palaeogeography Palaeoclimatology Palaeoecology 211, 325–344.

Malinverno, A., Erba, E., Herbert, T.D. 2010. Orbital tuning as an inverse problem: Chronology of the early Aptian oceanic anoxic event 1a (Selli Level) in the Cismon APTICORE. Paleoceanography 25, PA2203. doi:10.1029/2009PA001769.

Marshall, J.D., 1992. Climatic and oceanographic isotopic signals from the carbonate rock record and their preservation. Geologic Magazine 129, 143–160.

Méhay, S., Keller, C.E., Bernasconi, S.M., Weissert, H., Erba, E., Bottini, C., Hochuli, P.A., 2009. A volcanic CO_2 pulse triggered the Cretaceous Oceanic Anoxic Event 1a and a biocalcification crisis. Geology 37, 819–822.

Menegatti, A.P., Weissert, H., Brown, R.S., Tyson, R.V., Farrimond, P., Strasser, A., Caron, M., 1998. High resolution $\delta^{13}C$ stratigraphy through the early Aptian "Livello Selli" of the Alpine Tethys. Paleoceanography 13, 530–545.

Michalík, J., Soták, J., Lintnerová, O., Halásová, E., Bak, M., Skupien, P., Boorová, D., 2008. The stratigraphic and paleoenvironmental setting of Aptian OAE black shale deposits in the Pieniny Klippen Belt, Slovak Western Carpathians. Cretaceous Research 29, 871–892.

Millán, M.I., Weissert, H.J., Fernández-Mendiola, P.A., García-Mondéjar, J., 2009. Impact of early Aptian carbon cycle perturbations on evolution of a marine shelf system in the Basque-Cantabrian Basin (Aralar, N Spain). Earth and Planetary Sciences Letters 287, 392–401.

Muller, R.A., MacDonald, J.G., 2000. Ice ages and astronomical causes: data, spectral analysis, and mechanisms. Springer Praxis, Berlin.

Mutterlose, J., Bornemann, A., Herrle, J., 2009. The Aptian–Albian cold snap: evidence for "mid" Cretaceous icehouse interludes. Neues Jahrbuch für Geologie und Paläontologie Abhandlungen 252, 217–225.

Najarroa, M., Rosalesa, I., Moreno-Bedmarb, J.A., de Geac, G.A., Barróna, E., Companyd, M., Delanoye, G., 2011. High-resolution chemo- and biostratigraphic records of the early Aptian oceanic anoxic event in Cantabria (N Spain): Palaeoceanographic and palaeoclimatic implications. Palaeogeography, Palaeoclimatology, Palaeoecology 229, 137–158.

Okay, A.I., Tuysuz, O., 1999. Tethyan sutures of northern Turkey. In: Durand, B., Jolivet, L., Horvath, E., Seranne, M. (Eds.), The Mediterranean Basins: Tertiary Extension within the Alpine Orogen. Geological Society, London, Special Publications 56, pp. 475–515.

Sengor, A.M.C., Yilmaz, Y., 1981. Tethyan evolution of Turkey, a plate tectonic approach. Tectonophysics 75, 181–241.

Schlanger, S.O., Jenkyns, H.C., 1976. Cretaceous oceanic anoxic events: causes and consequences. Geologie en Mijnbouw 55, 179–184.

Stein, M., Föllmi, K.B., Westermann, S., Godet, A., Adatte, T., Matera, V., Fleitmann, D., Berner, Z., 2011. Progressive palaeoenvironmental change during the late Barremian-early Aptian as prelude to Oceanic Anoxic Event 1a: Evidence from the Gorgo a Cerbara section (Umbria-Marche basin, central Italy). Palaeogeography Palaeoclimatology Palaeoecology 302, 396–406.

Tejada, M.L.G., Suzuki, K., Kuroda, J., Coccioni, R., Mahoney, J.J., Ohkouchi, N., Sakamoto, T., Tatsumi, Y., 2009. Ontong Java Plateau eruption as a trigger for the early Aptian oceanic anoxic event. Geology 37, 855–858.

van Breugel, Y., Schouten, S., Tsikos, H., Erba, E., Price, G. D., Sinninghe Damste J.S., 2007. Synchronous negative carbon isotope shifts in marine and terrestrial biomarkers at the onset of the early Aptian oceanic anoxic event 1a: Evidence for the release of ^{13}C-depleted carbon into the atmosphere. Paleoceanography 22, PA1210. doi:10.1029/2006PA001341.

Wagner, T., Wallmann, K., Herrle, J.O., Hofmann, P., Stüsser, I., 2007. Consequences of moderate ~25,000 yr lasting emission of light CO_2 into the Mid-Cretaceous ocean. Earth and Planetary Science Letters 259, 200–211.

Wagreich, M., Neuhuber, S., Egger, J., Wendler, I., Scott, R.W., Malata, E., Sanders, D., 2009. Stratigraphy and facies of Cretaceous oceanic red beds (CORBs) in the Eastern Alps (Austria): pelagic passive margin vs. active margin depositional settings. In: Hu, X.M., Wang, C.S., Scott, R.W., Wagreich, M., Jansa, L. (Eds.), Cretaceous Oceanic Red Beds: Stratigraphy, Composition, Origins and Paleoceanographic and Paleoclimatic Significance. SEPM Special Publication 91, pp. 73–88.

Wagreich, M., Hu, X.M., Sageman, B., 2011. Causes of oxic–anoxic changes in Cretaceous marine environments and their implications for Earth systems—An introduction. Sedimentary Geology 235, 1–4.

Wang, C.S., Huang, Y.J., Hu, Y.M., Li, X.H., 2004. Cretaceous oceanic redbeds: implications for paleoclimatology and paleoceanography. Acta Geologica Sinica-English Edition 78 (3), 873–877.

Wang, C., Hu, X., Sarti, M., Scott, R.W., Li, X., 2005. Upper Cretaceous oceanic red beds in southern Tibet: a major change from anoxic to oxic, deep-sea environments. Cretaceous Research 26, 21–32.

Wang, C., Hu, X., Huang, Y., Scott, W., Wagreich, M., 2009. Overview of the Cretaceous Oceanic Red Beds (CORBs): a window on Global Oceanic/Climate Change. In: Hu, X.M., Wang, C.S., Scott, R.W., Wagreich, M., Jansa, L. (Eds.), Cretaceous Oceanic Red Beds: Stratigraphy, Composition, Origins and Paleoceanographic and Paleoclimatic Significance. SEPM Special Publication 91, pp. 13–33.

Wang, C., Hu, X., Huang, Y., Wagreich, M., Scott, R., Hay, W., 2011. Cretaceous oceanic red beds as possible consequences of oceanic anoxic events. Sedimentary Geology 235, 27–37.

Weedon, G., 2003. Time-series analysis and cyclostratigraphy. Cambridge University Press.

Weissert, H., Erba, E., 2004. Volcanism, CO_2 and palaeoclimate: a Late Jurassic–Early Cretaceous carbon and oxygen isotope record. Journal of the Geological Society London 161, 695–702.

Weissert, H., Lini, A., 1991. Ice age interludes during the time of Cretaceous greenhouse climate? In: Müller, D.W., McKenzie, J.A., Weissert, H. (Eds.), Controversies in Modern Geology. Academy Press, London, pp. 171–191.

Yilmaz, I.O., 2008. Cretaceous Pelagic Red Beds and Black Shales (Aptian - Santonian), NW Turkey: Global Oceanic Anoxic and Oxic Events. Turkish Journal of Earth Sciences 17, 263–296.

Yilmaz, I.O., Vennemann, T., Altiner, D., Satir, M., 2004. Stable isotope evidence for meter-scale sea level changes in lower Cretaceous inner platform and pelagic carbonate successions of Turkey. Geologica Carpathica 55, 19–36.